Available online at www.sciencedirect.com

SciVerse ScienceDirect

Ceramics International 39 (2013) 431–437

CERAMICS INTERNATIONAL

www.elsevier.com/locate/ceramint

New morphological $Ba_{0.5}Sr_{0.5}Co_{0.8}Fe_{0.2}O_{3-\alpha}$ hollow fibre membranes with high oxygen permeation fluxes

Dezhi Han[a,c], Xiaoyao Tan[b], Zifeng Yan[a,*], Qin Li[c], Shaomin Liu[c,**]

[a]State Key Laboratory of Heavy Oil Processing, CNPC Key Laboratory of Catalysis, China University of Petroleum, Qingdao 266555, China
[b]School of Chemical Engineering, Shandong University of Technology, Zibo 255049, China
[c]Department of Chemical Engineering, Curtin University, Perth, WA 6845, Australia

Received 23 April 2012; received in revised form 14 June 2012; accepted 14 June 2012
Available online 21 June 2012

Abstract

Perovskite $Ba_{0.5}Sr_{0.5}Co_{0.8}Fe_{0.2}O_{3-\alpha}$ (BSCF) hollow fibre membranes were fabricated by a combined phase inversion and sintering technique. The membranes were characterised by XRD, SEM and tested for air separation. The membrane possesses a novel morphology consisting of one dense layer and one porous layer. Oxygen permeation fluxes through the obtained hollow fibre membranes were measured in the temperature range 650–950 °C using helium sweep gas rates from 50 to 200 mL min^{-1}. Experimental results indicated the oxygen permeation flux through the BSCF hollow fibre membrane sintered at 1050 °C was approximately 11.46 mL min^{-1} cm^{-2} at 950 °C when the helium sweep rate was kept at 200 mL min^{-1}. The BSCF hollow fibre membrane showed a stable oxygen permeation flux of 8.60 mL min^{-1} cm^{-2} over the investigated period of 120 h at 900 °C.

Keywords: Air separation; Hollow fibre; Inorganic membrane; Perovskite

1. Introduction

Oxygen permeation phenomena through mixed ionic–electronic conducting (MIEC) membranes have attracted considerable attention due to their wide research interest in oxygen production, membrane reactors for high temperature oxidations and solid oxide fuel cells [1–10]. The increasing awareness of reducing greenhouse gas emissions has resulted in the development of new technologies in clean energy delivery with lower carbon dioxide emission [11]. Among these technologies, oxyfuel combustion is a promising option due to its possibility of integrating but not demolishing the existing facilities of the coal/gas fired-power stations [12]. Several big projects have been initiated in the world such as CS Callide (Australia), Vattenfal (Germany), Inabensa (Spain), OXY-CFB-300 (Spain), TotalLacq (France) and the FutureGen2 (USA) programme with billion dollar investments for each of these projects [13]. With the oxyfuel concept, coal will be fired with pure O_2 or an O_2/CO_2 mixture instead of air; in this case, the major constituent of the flue gas produced would be highly concentrated CO_2 enabling its capture to become more economically feasible. Coupling an MIEC membrane unit for air separation at the front end of an oxyfuel power plant offers the potential to tackle the energy penalties which result from the conventional cryogenic method to produce oxygen, thus improving the viability of CO_2 zero emission technology. Due to these potentials, the intensive research in MIEC membranes has been directed to two major areas addressing the oxygen fluxes and membrane stability under real application conditions. This paper addresses the oxygen flux improvement by the development of a new morphological membrane. Two typical materials attracting most attention in theoretical and experimental studies are $Ba_{0.5}Sr_{0.5}Co_{0.8}Fe_{0.2}O_{3-\alpha}$ (BSCF) and $La_{0.6}Sr_{0.4}Co_{0.2}Fe_{0.8}O_{3-\alpha}$ (LSCF). BSCF membrane is well known for its higher oxygen flux but LSCF is characterised by its good material stability and mechanical strength [1,2,4]. Normally, perovskite membranes with large thickness (>1 mm) give relatively low oxygen fluxes due to their ionic transport and surface transferring reaction limitations [1,14].

*Corresponding author. Tel.: +86 532 86981296; fax: +86 532 86981295.
**Corresponding author. Tel.: +61 8 92669056.
E-mail addresses: zfyancat@upc.edu.cn (Z. Yan), shaomin.liu@curtin.edu.au (S. Liu).

0272-8842/$36.00
http://dx.doi.org/10.1016/j.ceramint.2012.06.044

The improvement strategy lies in the membrane thickness reduction [15,16], surface area increase [17–19] and additional catalyst integration [20–23]. Conventional thin membrane technology can be used to reduce the thickness via coating methods using a porous support, but the procedure is normally multi-step and time-consuming [24]. Most previous work employed membranes in the form of discs or tubes which are easily fabricated using conventional methods [1,14,25]. However, these geometries do not meet the requirements for industrial applications because of their low effective surface area to the volume ratio and low oxygen permeation flux due to the large gas transport resistance through the thick membrane. Asymmetric hollow fibre membranes seem to overcome these shortcomings perfectly by not only providing a thinner gas transport layer for more interesting fundamental studies but also providing a larger membrane area per unit volume with easy sealing for favourable scaling up [22,23,26]. More importantly, these ceramic hollow fibre membranes with favourable structure can be completed in one sintering step. The hollow fibre precursor can be produced via a room temperature spinning (or extrusion) process based on phase inversion principles. Previously, based on polyethersulfone (PESf)/N-methyl-2-pyrrolidone (NMP) as the binder and water as the coagulants, BSCF hollow fibre with a thickness of 200 μm was prepared and the oxygen flux up to 5.1 mL min^{-1} cm^{-2} at 950 °C was achieved [2]. Later, a new sulphur-free polymer of polyetherimide (PEI) was used to replace the PESF to avoid the sulphur contamination of the membrane material and the oxygen flux was improved to 9.5 mL min^{-1} cm^{-2} at 950 °C under the oxygen partial pressure gradient created by air and sweep gas [23]. However, when water is used for internal and external coagulant, normally the ceramic hollow fibre membrane would possess an asymmetric structure consisting of three dense layers and two porous layers full of isolated short finger-like pores near the inside and outside surfaces. When gas is transported through such MIEC membranes with these isolated pores, it will encounter greater transport resistance [16,27]. A more densified structure with the decrease or removal of these isolated pores will definitely improve the BSCF membrane performance in terms of oxygen flux and mechanical strength. In this paper, we report an improved method to prepare the BSCF hollow fibre membranes by making a minor change in the conventional internal coagulant composition used during the spinning process. The resultant BSCF membrane has a new morphology and further improves the oxygen flux by approximately 30% at 950 °C, which exceeds the commercial target of 10 mL min^{-1} cm^{-2} [28,29].

2. Experimental

$Ba_{0.5}Sr_{0.5}Co_{0.8}Fe_{0.2}O_{3-\alpha}$ (BSCF) perovskite powders were derived from a combined EDTA-citrate sol–gel method using the appropriate nitrates [2]. The prepared oxide powder was ball-milled for 48 h in an agate jar and sieved through a 200-mesh sieve. The BSCF powder was added to a mixture of solvent (N-methyl-2-pyrrolidinone (NMP)) and polyetherimide (PEI) in the ratio of 6:1:4 (w/w) to create the spinning dope. The mixture was constantly stirred for a period of 24 h to ensure a uniform mixture. The viscosity of the mixture was adjusted by adding a minor amount ($<1\%$, w/w) of polyvinyl pyrrolidinine (PVP) and measured at room temperature to be around 55,800 mPa s at a shear rate of 3 rpm for easy spinning. The bore fluid as the internal coagulant was a mixture of 30 wt% ethanol-70 wt% NMP while tap water was used normally as the external coagulant. The dope mixture was extruded via a tube-in-orifice spinneret (OD = 2.5 mm and ID = 0.8 mm) into thin hollow fibres which were gelled by immersion in tap water. Subsequently, the extruded BSCF hollow fibres were dried, cut in short lengths of 12 cm, and sintered at 1050 °C or 1100 °C for 4 h with a ramping and cooling rate of 2 °C min^{-1} in non-flowing air atmosphere to obtain gas-tight membranes.

The oxygen permeation was tested by suspending a gas tight hollow fibre between two quartz tubes in a tubular furnace and exposing the outside surface to ambient air with helium as sweep gas on the lumen side. Prior to the assembly, the gas tightness of the hollow fibre was checked by observing whether or not there was any bubble appearing from the outside surface of the hollow fibre, which was immersed into a water bath with lumen side applied by a compressed air up to 2 bar. High temperature permeation experiments were conducted by varying the helium gas flow rate between 50 and 200 ml min^{-1} and the temperature between 650 and 950 °C. The permeate stream was analysed online using a Shimadzu GC-2014 with a 5A molecular sieve column and TCD detector. The permeate flow rate was measured by a bubble flow metre. The hollow fibres were sealed with silver paste and resealed at least twice until nitrogen could no longer be detected by gas chromatography. The air leak rate was $<0.5\%$, below the minimum detection limit of the Shimadzu GC-2014. The effective membrane area was calculated using the following equation:

$$A = \frac{2\pi L(r_o - r_i)}{\ln(r_o/r_i)}$$

where A, L, r_o and r_i stand for the effective membrane area, the effective length of the hollow fibre sample, the outer and the inner radius of the hollow fibre, respectively.

Viscosity of the spinning solutions were measured by a Physica UDS-200 rheometer at room temperature. Morphology and microstructures of the hollow fibre membranes were observed using scanning electron microscopy (SEM) (Zeiss EVO 40XVP). Gold sputter coating was performed on the samples under vacuum before the measurement. The XRD patterns were recorded on an X-ray diffractometer (PANalytical X'Pert PRO MPD) using a Cu-Kα monochromatized radiation source and a Ni filter in the range 2θ from 10 to 80°.

3. Results and discussion

The XRD spectra of the BSCF hollow fibres membrane sintered at 1050 °C shown in Fig. 1 exhibited the anticipated

patterns of the pure perovskite phase characterised with several strong diffraction peaks of the respective 2θ angles and lattice planes of 22.35 (100), 31.87 (110), 39.25 (111), 45.60 (200), 51.30 (210), 56.60 (211), 66.35 (220) and 75.70 (310). SEM images of the BSCF hollow fibre precursors are shown in Fig. 2. The typical outer and inner diameter of the fibre precursors are around 2.90 and 1.90 mm, respectively, as measured from Fig. 2(A). A further inspection of Fig. 2(B) shows the presence of short finger-like porous structures at outer side surface (marked with red box), while a sponge-like structure exists in the inner side of the precursor. The formation of this asymmetric structure is attributed to the polymer phase inversion process. Normally, when water is used for both the internal or external coagulants, there are two layers of finger-like pore arrays [23,26]. In the current case, the internal coagulant is replaced by 30 wt% ethanol-70 wt% NMP, which was previously used to produce honeycomb-structured LSCF hollow fibres [27]. Due to the presence of high concentrated NMP, the NMP transport rate from the polymer phase had been slowed down compared to the water as the internal coagulant. Therefore, a sponge-like structure near the inner surface was produced. Nonetheless, a rapid precipitation still occurred at outer side surface resulting in short finger-like pores. Fig. 2(C) and (D) shows the inner and outer surface views of the hollow fibre precursor, from which can be observed that the BSCF particles were well dispersed and connected to each other by the polymer binder.

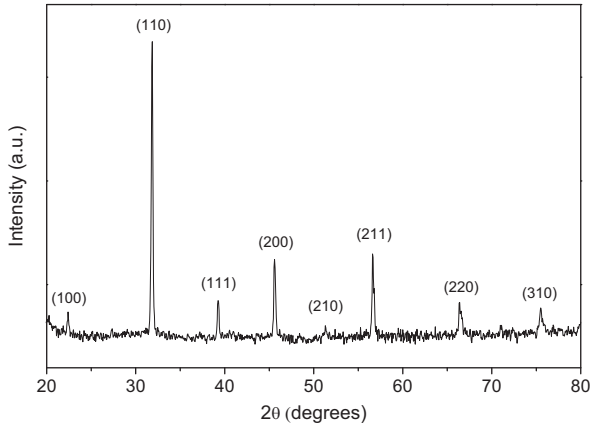

Fig. 1. Typical XRD patterns of the BSCF hollow fibre sintered at 1050 °C.

Fig. 3 shows the SEM images of BSCF hollow fibre membranes sintered at different temperatures. The hollow fibre was sintered at 1050 °C resulting in the wall thickness of 300 μm and the outer diameter of 1.64 mm (Fig. 3(A)). A magnified section of the hollow fibre wall illustrates the general morphology of the fibre precursor was maintained after sintering. However, the fibre only possessed one dense layer near the inner surface (marked with a black box in Fig. 3(B)) and one porous layer with the finger-like pores near the outer surface (marked with a red box in Fig. 3(B)). The micrograph of Fig. 3(C) relates to the hollow fibre's inner surface showing complete densification with the growth of large grain size. However, relatively uniform pin holes are clearly observed at the outer surface (Fig. 3(D)) particularly from the inserted image. These pin holes are the open ends of these finger-like pores near the outside surface, which would facilitate the molecular oxygen transferring to lattice oxygen via surface reactions at air side. After sintering at 1100 °C, it can be seen that both the inner and outer surface of the hollow fibre become more densified (Fig. 3(E) and (F)) and most of

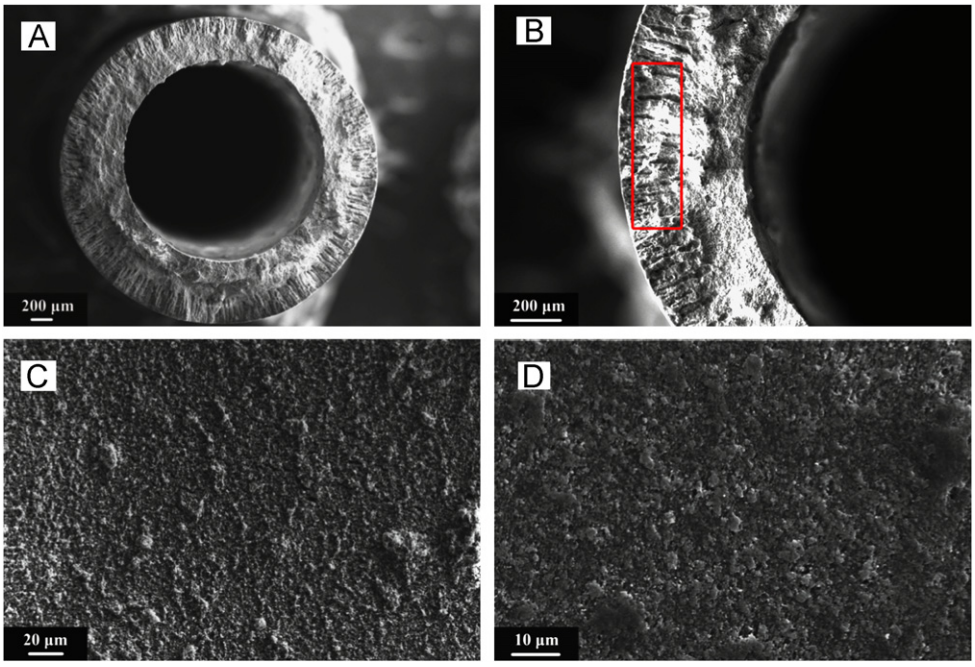

Fig. 2. SEM images of BSCF hollow fibre precursor (A) cross sectional view; (B) fibre wall; (C) inner surface; (D) outer surface.

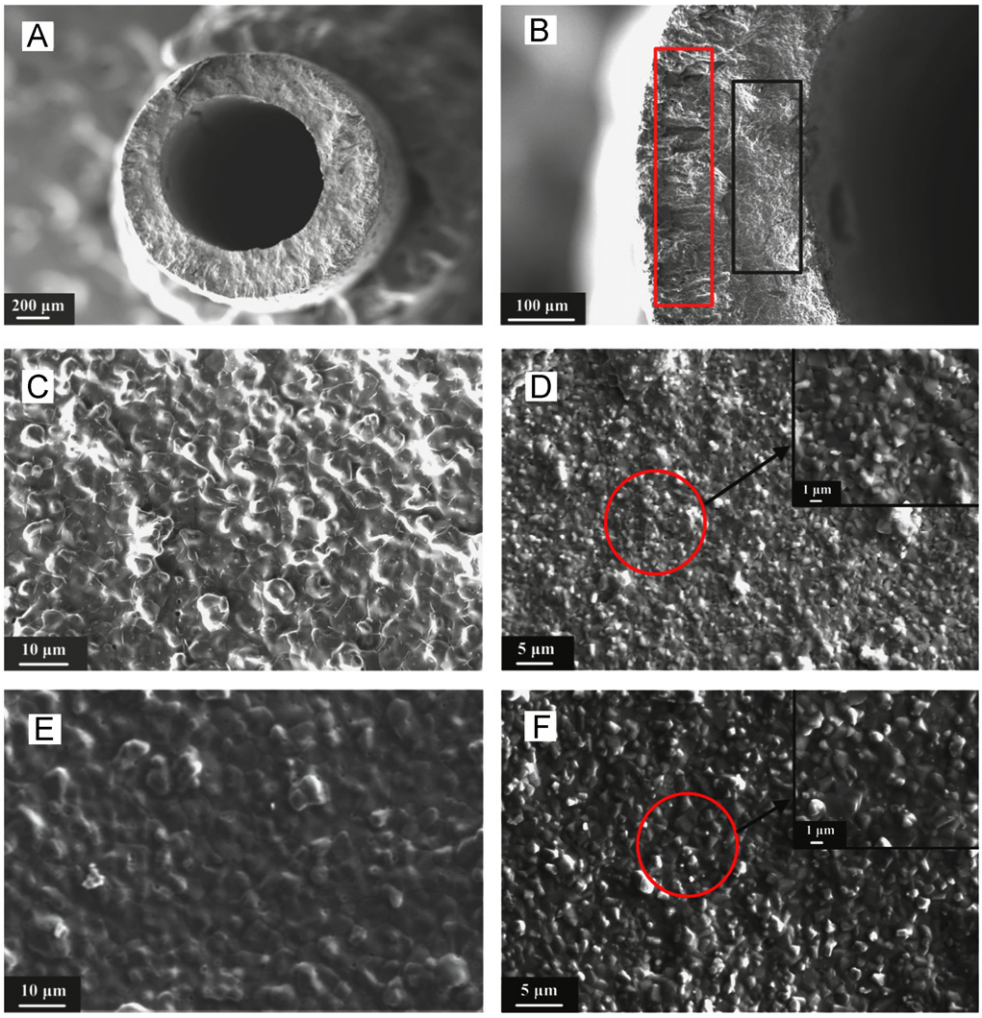

Fig. 3. SEM images of BSCF hollow fibre sintered at 1050 °C ((A)–(D)) and 1100 °C ((E) and (F)) (A) cross sectional view; (B) fibre wall; ((C) and (E)) inner surface; ((D) and (F)) outer surface. (For interpretation of the references to color in this figure, the reader is referred to the web version of this article.)

the finger-like pores became isolated and were trapped inside the membrane increasing the oxygen permeation resistance. When the membrane was sintered at temperatures lower than 1050 °C (i.e., 1000 °C), the membrane could not reach the gas-tightness properties due to the decreased densification and the achieved mechanical strength was too weak to be routinely handled.

Fig. 4 presents the oxygen permeation fluxes against temperatures. The used BSCF hollow fibre samples were sintered at 1050 and 1100 °C, respectively. The oxygen fluxes increased steadily with the temperature due to the enhancement of oxygen ionic bulk-diffusion and the surface-exchange reaction rates. For instance, the oxygen fluxes through the BSCF membrane sintered at 1050 and 1100 °C rose from 1.98 to 9.92 and 1.38 to 8.11 mL min^{-1} cm^{-2}, respectively, as the operating temperature increased from 750 to 950 °C at the sweep gas rate of 100 mL min^{-1}. We also observed that at similar operating conditions, the BSCF membrane sintered at 1050 °C provided much higher fluxes than that of the membrane sintered at

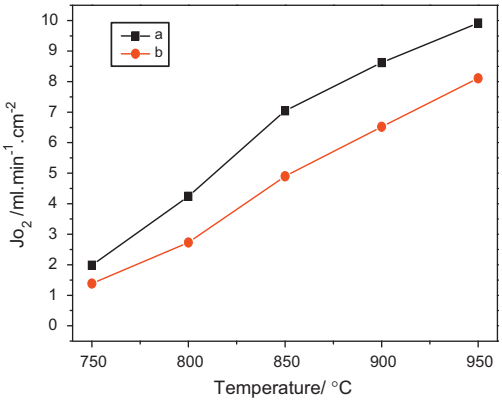

Fig. 4. Oxygen permeation fluxes through BSCF hollow fibres sintered at 1050 °C (a) and 1100 °C (b).

1100 °C, which is in a good agreement of the previous analysis of the membrane morphology as shown in Fig. 3. The better oxygen flux value achieved by the sample

sintered at 1050 °C is contributed by its unique membrane morphology with one dense layer integrated on the porous structure which is favourable for oxygen permeation. Fig. 5 shows the oxygen permeation fluxes against sweep gas flow rates at different operating temperatures. The BSCF membrane sintered at 1050 °C provided very high oxygen permeation flux up to 11.46 mL min^{-1} cm^{-2} with a helium sweep rate of 200 ml min^{-1} at 950 °C. This flux exceeded the previously reported results of BSCF [23] and BCFZ [30] hollow fibre of 9.5 and 7.6 mL min^{-1} cm^{-2}, respectively. In principle, the changes on the sweep gas rate which affect the driving force associated with the concentration gradient of oxygen should translate into the variations of the oxygen fluxes though the hollow fibres. However, this is not entirely the case for both BSCF membranes. There is no significant increase of oxygen fluxes with increasing the helium sweep rate below 800 °C. For example, at 800 °C, increasing the sweep gas rate from 50 to 200 ml min^{-1} slightly raised the oxygen flux though the two membrane samples from 3.90 to 4.36 and 2.45 to 2.84 mL min^{-1} cm^{-2}, respectively. On the other hand, the expected increase of oxygen flux as a function of the sweep gas rate occurred for temperatures above 800 °C. For instance, the oxygen flux though the two BSCF membranes increased dramatically from 8.22 to 11.46 and 6.28 to 9.71 mL min^{-1} cm^{-2}, respectively, as the sweep gas rate increased from 50 to 200 ml min^{-1} at 950 °C. Similar phenomenon was observed by other researchers [31]. The significantly different effects of sweep gas rate on the oxygen flux values under different temperatures indicating the driving force for oxygen transport through the MIEC membranes is not only related to oxygen concentration gradient but also related to temperature. In other words, the operating temperature plays a more important role in oxygen permeation than the concentration driving force for oxygen permeation in BSCF membranes. For example, at room temperature, no matter how the oxygen concentration in the permeate side varies, the oxygen transportation phenomenon would never be observed; otherwise, it would become another example of a perpetual motion machine. The observed oxygen flux of 11.46 mL min^{-1} cm^{-2} at 950 °C is the best value among the current literatures of mixed conducting membranes at relatively similar operating conditions like air as the feed gas and inert gas as the sweep gas. Noteworthy that membrane performance comparison should be made under relatively similar conditions. Certainly the flux value of the currently investigated membrane can be further improved if additional catalyst is applied on the membrane surface or the membrane is operated at other conditions like higher temperature environments, highly pressurised pure oxygen as feed gas or the exposure of the membrane permeate side to reactions to create a super-lower oxygen partial pressure zone where the permeated oxygen is consumed by oxidation. Baumann et al. reported the flux of 70 μ-thick-BSCF membrane up to 67.7 mL min^{-1} cm^{-2} at 1000 °C when operated under these extreme conditions [32]. A long-term

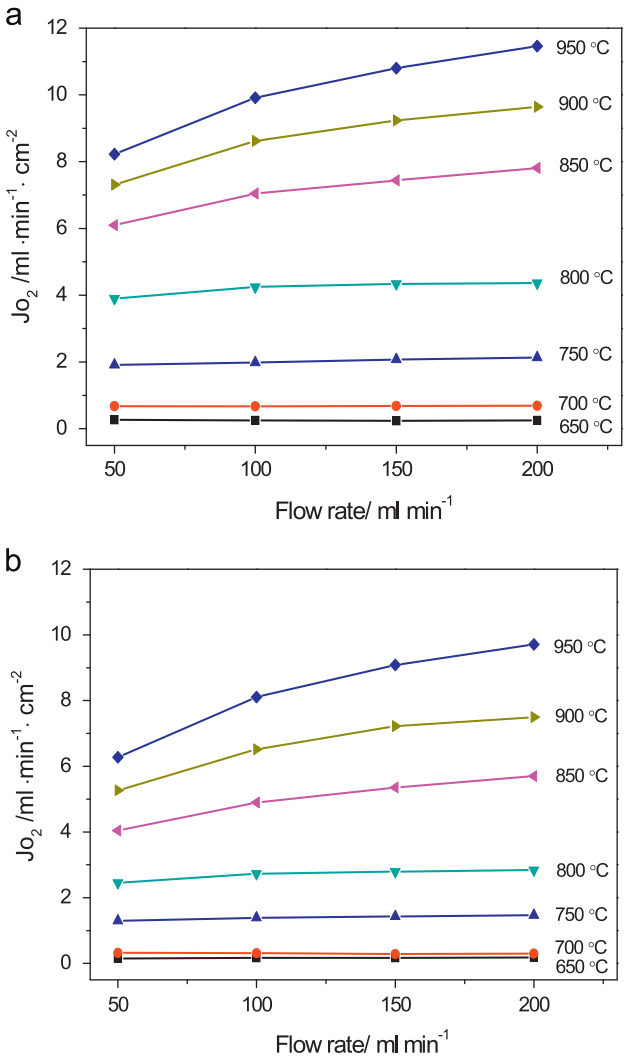

Fig. 5. Effects of helium sweep rate on the oxygen fluxes through the BSCF hollow fibre membranes sintered at 1050 °C (a) and 1100 °C (b).

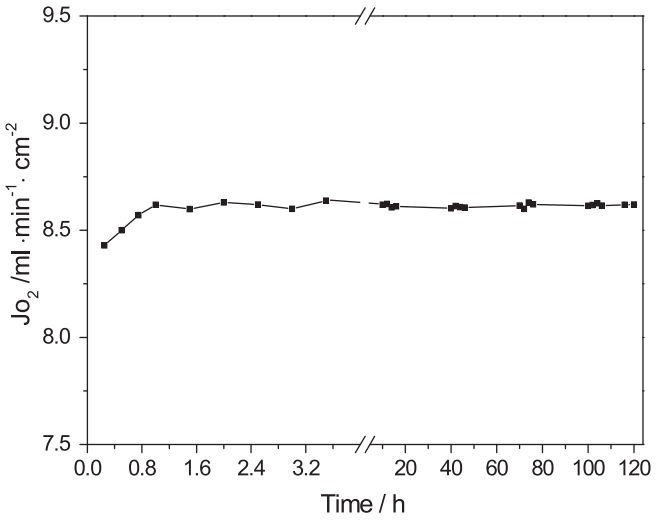

Fig. 6. Oxygen permeation flux through the BSCF hollow fibre sintered at 1050 °C as function of operation time at 900 °C.

operation test was also conducted on the BSCF hollow fibre sintered at 1050 °C under the operating conditions of 900 °C and 100 ml min^{-1} sweep gas rate. The oxygen permeation flux plotted against operation time is shown in Fig. 6. As observed, within 1 h after the sweep gas was introduced, the membrane system reached steady state and gave a stable oxygen flux value of 8.60 mL min^{-1} cm^{-2} for the entire operation period of 120 h at 900 °C. This implies that the BSCF membrane sintered at 1050 °C shows high stability at least under the investigated operational conditions.

4. Conclusions

The gas-tight $Ba_{0.5}Sr_{0.5}Co_{0.8}Fe_{0.2}O_{3-\alpha}$ (BSCF) hollow fibre membranes with an asymmetric structure were fabricated by spinning a polymer solution containing BSCF powders followed by sintering at 1050 or 1100 °C for 4 h. With a new composition of the internal coagulant used for the hollow fibre precursor formation process, the prepared BSCF membrane possesses a novel morphology favourable for oxygen transport. The BSCF hollow fibre membrane sintered at 1050 °C gave the best oxygen permeation flux values up to 11.5 mL min^{-1} cm^{-2} at 950 °C. Among the tested MIEC membranes without additional catalyst, so far this is the highest oxygen flux being observed, which exceeds the commercial target of at least 10 mL min^{-1} cm^{-2}. The prepared membrane also exhibited high oxygen permeation stability for the entire investigated 120 h-operation at 900 °C without flux decay.

Acknowledgements

The authors gratefully acknowledge the research funding provided by the Australian Research Council (DP 0878849 and DP0985578).

References

[1] Z. Shao, W. Yang, Y. Cong, H. Dong, J. Tong, G. Xiong, Investigation of the permeation behavior and stability of a $Ba_{0.5}Sr_{0.5}Co_{0.8}Fe_{0.2}O_{3-\alpha}$ oxygen membrane, Journal of Membrane Science 172 (2000) 177–188.

[2] S. Liu, G.R. Gavalas, Oxygen selective ceramic hollow fibre membranes, Journal of Membrane Science 246 (2005) 103–108.

[3] S.P.S. Badwal, F.T. Ciacchi, Ceramic membrane technologies for oxygen separation, Advanced Materials 13 (2001) 993–996.

[4] X. Tan, K. Li, Oxidative coupling of methane in a perovskite hollow fibre membrane reactor, Industrial and Engineering Chemistry Research 45 (2006) 142–149.

[5] H. Jiang, H. Wang, S. Werth, T. Schiestel, J. Caro, Simultaneous production of hydrogen and synthesis gas by combing water splitting with partial oxidation of methane in a hollow fibre membrane reactor, Angewandte Chemie International Edition 47 (2008) 9341–9344.

[6] F.T. Akin, Y.S. Lin, Selective oxidation of ethane to ethylene in a dense tubular membrane reactor, Journal of Membrane Science 209 (2002) 457–467.

[7] H.H. Wang, Y. Cong, W.S. Yang, High selectivity of oxidative dehydrogenation of ethane to ethylene in an oxygen permeable membrane reactor, Chemical Communications 14 (2002) 1468–1469.

[8] H.Y. Tu, Y. Takeda, N. Imanishi, O. Yamamoto, $Ln_{1-x}Sr_xCoO_3$ (Ln=Sm, Dy) for the electrode of solid oxide fuel cells, Solid State Ionics 100 (1997) 283–288.

[9] Z. Shao, S. Haile, High performance cathode for next-generation solid-oxide fuel cells, Nature 431 (2004) 170–173.

[10] G.J. Stiegel, R.C. Maxwell, Gasification technologies: the path to clean, affordable energy in the 21st century, Fuel Processing Technology 71 (2001) 79–97.

[11] D. Bücker, D. Holmberg, T. Griffin, Techno-Economic Evaluation of an Oxyfuel Power Plant Using Mixed Conducting Membranes, in Carbon Dioxide Capture for Storage in Deep Geologic Formations, Elsevier Science, Amsterdam, 2005, pp. 537–559.

[12] B.J.P. Buhre, L.K. Elliott, C.D. Sheng, R.P. Gupta, T.F. Wall, Oxy-fuel combustion technology for coal-fired power generation, Progress in Energy and Combustion Science 31 (2005) 283–307.

[13] C. Spero, Callide Oxyfuel Project: Feasibility Study, Report in Cooperative Research Centre for Coal in Sustainable Development, 2007.

[14] H. Wang, Y. Cong, W.S. Yang, Oxygen Permeation Study in a Tubular $Ba_{0.5}Sr_{0.5}Co_{0.8}Fe_{0.2}O_{3-\delta}$, Journal of Membrane Science 210 (2002) 259–271.

[15] H. Liu, X. Tan, Z. Pang, J.C. Diniz da Costa, G.Q. Lu, S. Liu, Novel dual structured mixed conducting ceramic hollow fibre membranes, Separation and Purification Technology 63 (2008) 243–247.

[16] Z. Wang, H. Liu, X. Tan, Y. Jin, S. Liu, Improvement of the oxygen permeation through perovskite hollow fibre membranes by surface acid-modification, Journal of Membrane Science 345 (2009) 65–73.

[17] J.P. Kim, J.H. Park, E. Magnone, Y. Lee, Significant improvement of the oxygen permeation flux of tubular $Ba_{0.5}Sr_{0.5}Co_{0.8}Fe_{0.2}O_{3-\delta}$ membranes covered by a thin $La_{0.6}Sr_{0.4}Ti_{0.3}Fe_{0.7}O_{3-\delta}$ layer, Materials Letters 65 (2011) 2168–2170.

[18] T. Kida, S. Ninomiya, K. Watanabe, N. Yamazoe, K. Shimanoe, High oxygen permeation in $Ba_{0.95}La_{0.05}FeO_{3-\delta}$ membranes with surface modification, ACS Applied Materials and Interfaces 2 (10) (2010) 2849–2853.

[19] S. Lee, K.S. Lee, S.K. Woo, J.W. Kim, T. Ishihara, D.K. Kim, Oxygen-permeating property of $LaSrBFeO_3$ (B=Co, Ga) perovskite membrane surface-modified by $LaSrCoO_3$, Solid State Ionics 158 (2003) 287–296.

[20] A. Leo, S. Liu, J.C. Diniz da Costa, The enhancement of oxygen flux on $Ba_{0.5}Sr_{0.5}Co_{0.8}Fe_{0.2}O_{3-\alpha}$ (BSCF) hollow fibers using silver surface modification, Journal of Membrane Science 340 (2009) 148–153.

[21] A. Leo, S. Liu, J.C. Diniz da Costa, Production of pure oxygen from BSCF hollow fibre membranes using steam sweep, Separation and Purification Technology 78 (2011) 220–227.

[22] X. Tan, Z. Wang, H. Liu, S. Liu, Enhancement of oxygen permeation through $La_{0.6}Sr_{0.4}Co_{0.2}Fe_{0.8}O_{3-\alpha}$ hollow fibre membranes by surface modifications, Journal of Membrane Science 324 (2008) 128–135.

[23] A. Leo, S. Smart, S. Liu, J.C. Diniz da Costa, High performance perovskite hollow fibres for oxygen separation, Journal of Membrane Science 368 (2011) 64–68.

[24] S. Battersby, S. Smart, B. Ladewig, S. Liu, M. Duke, V. Rudolph, J.C. Diniz da Costa, Hydrothermal stability of cobalt silica membranes in a water gas shift membrane reactor, Separation and Purification Technology 66 (2009) 299–305.

[25] J.E. ten Elshof, H.J.M. Bouwmeester, H. Verweij, Oxidative coupling of methane in a mixed-conducting perovskite membrane reactor, Applied Catalysis A: General 130 (1995) 195–212.

[26] S. Liu, X. Tan, Z. Shao, J.C. Diniz da Costa, $Ba_{0.5}Sr_{0.5}Co_{0.8}Fe_{0.2}O_{3-\delta}$ ceramic hollow fibre membranes for oxygen permeation, AIChE Journal 52 (2006) 3452–3461.

[27] N. Liu, X. Tan, B. Meng, S. Liu, Honeycomb-structured perovskite hollow fibre membranes with ultra-thin densified layer for oxygen separation, Separation and Purification Technology 80 (2011) 396–401.

[28] K. Watenabe, M. Yuasa, T. Kida, Y. Teraoka, N. Yamazoe, K. Shimanoe, High-performance oxygen-permeable membranes with an asymmetric structure using $Ba_{0.95}La_{0.05}FeO_{3-\alpha}$ perovskite-type oxide, Advanced Materials 22 (2010) 2367–2370.

[29] Technical report for Development of Hydrogen-Manufacturing Technology from Steel-Making By-Product Gases; The Japan Research and Development Center for Metals, Foundation: Tokyo, 2006.
[30] T. Schiestel, M. Kilgus, S. Peter, K.J. Caspary, H. Wang, J. Caro, Hollow fibre perovskite membranes for oxygen separation, Journal of Membrane Science 258 (2005) 1–4.
[31] J. Sunarso, S. Liu, Y.S. Lin, J.C. Diniz da Costa, High performance BaBiScCo hollow fibre membranes for oxygen transport, Energy and Environmental Science 4 (2011) 2516–2519.
[32] S. Baumanna, J.M. Serrab, M.P. Loberab, S. Escolásticob, F. Schulze-Küppersa, W.A. Meulenberg, Ultrahigh oxygen permeation flux through supported $Ba_{0.5}Sr_{0.5}Co_{0.8}Fe_{0.2}O_{3-\delta}$ membranes, Journal of Membrane Science 377 (2011) 198–205.